PSFC/JA-08-5

Study of direct-drive capsule implosions in inertial confinement fusion with proton radiography

C. K. Li, F. H. Séguin, J. R. Rygg, J. A. Frenje, M. Manuel, R. D. Petrasso
Plasma Science and Fusion Center, Massachusetts Institute of Technology, Cambridge, Massachusetts 02139, USA

V. A. Smalyuk, R. Betti[1], J. Delettrez, J. P. Knauer, F. Marshall, D. D. Meyerhofer[1], D. Shvarts[2], C. Stoeckl, and W. Theobald
Laboratory for Laser Energetics, University of Rochester, Rochester, New York 14623, USA
[1]also *Department of Mechanics Engineering, Physics and Astronomy, University of Rochester, Rochester, New York 14623, USA*
[2]also *NRCN, Negev and Ben Gurion University of the Negev, Beer-Sheva 84015, Israel*

O. L. Landen , R. P. J. Town and P. A. Amendt
Lawrence Livermore National Laboratory, Livermore, California 94550 USA

C. A. Back and J. D. Kilkenny
General Atomics, San Diego, California, 92186 USA

25 July 2008

Plasma Science and Fusion Center
Massachusetts Institute of Technology
Cambridge, MA 02139 USA

The work described here was performed in part at the LLE National Laser User's Facility (NLUF), and was supported in part by US DOE (Grant No. DE-FG03-03SF22691), LLNL (subcontract Grant No. B504974), and LLE (subcontract Grant No. 412160-001G).

Submitted to ***Plasma Physics and Controlled Fusion***

Study of direct-drive capsule implosions in inertial confinement fusion with proton radiography

C. K. Li[1], F. H. Séguin[1], J. R. Rygg[1], J. A. Frenje[1], M. Manuel[1], R. D. Petrasso[1], V. A. Smalyuk[1], R. Betti[2,3], J. Delettrez[2], J. P. Knauer[2], F. Marshall[2], D. D. Meyerhofer[2,3], D. Shvarts[2,4], C. Stoeckl[2], W. Theobald[2], O. L. Landen[5], R. P. J. Town[5], P. A. Amendt[5], C. A. Back[6] and J. D. Kilkenny[6]

[1] Plasma Science and Fusion Center, Massachusetts Institute of Technology, Cambridge, Massachusetts 02139 USA

[2] Laboratory for Laser Energetics, University of Rochester, Rochester, New York 14623 USA

[3] Department of Mechanical Engineering, Physics and Astronomy, University of Rochester, Rochester, New York 14623 USA

[4] NRCN, Negev and Ben Gurion University of the Negev, Beer-Sheva 84015 Israel

[5] Lawrence Livermore National Laboratory, Livermore, California 94550 USA

[6] General Atomics, San Diego, California 92186 USA

Abstract

Implosions of spherical and cone-in-shell targets in direct-drive inertial confinement fusion (ICF) are studied with proton radiography. Time-gated, 15-MeV proton images provide a unique and comprehensive picture of ICF implosions that cover all the implosion phases from acceleration, through coasting, deceleration, to stagnation. Observation and study have resulted in the discovery and characterization of self-generated internal radial electric fields, and the direction reversal of such fields during the course of implosions. Monte-Carlo simulations quantitatively confirm the observations of the electric field and its evolution. For further elucidation of these implosions, data is also contrasted using both self-emitted x rays and hydrodynamic simulations.

1. Introduction

Achieving ignition and high gain is the ultimate goal of inertial confinement fusion (ICF) [1-4], which requires that a cryogenic deuterium-tritium (DT) filled spherical capsule be symmetrically imploded to reach sufficiently high temperature and density. In the direct-drive approach to ICF, such an implosion occurs in response to a large number of high-power, individual laser beams illuminating the surface of a capsule [1-4]. There are currently two major schemes for target ignition which are being studied: the first, the conventional "hot spot" ignition scheme for which the formation of two different regions occurs as a consequence of capsule implosion: a small mass of low density, hot fuel at the center surrounded by a larger mass of high density, low temperature fuel. Shock coalescence "ignites" the hot spot, and a self-sustaining burn wave propagates into the main fuel region; The second approach to target ignition, the "fast ignition" scheme, involves a pre-compressed target being ignited by an external "spark". Since fast ignition separates capsule compression from hot spot formation, this method may potentially relax

the conditions on target compression and reduce the total energy requirements for ICF ignition, which could lead to higher target gain [5].

Successful ICF implosion requires the understanding and controlling of implosions dynamics, which have been studied experimentally with a number of diagnostics. Conventional x-ray diagnostics (the measurements of x rays from either self emission or backlighting [6,7]) are very valuable, but don't directly provide information about mass assembly [areal density (ρR)] or self-generated electric (E) and magnetic (B) fields. On the other hand, measurements of self-emitted fusion products, such as neutrons and charged particles, can provide information about conditions at nuclear bang time but are not very useful for studying dynamics earlier or later [8-11].

In this article we present unique nuclear observations of capsule implosions of direct-drive spherical and cone-in-shell targets on the OMEGA laser facility [12], using a novel method of monoenergetic proton radiography [13-18]. The combination of the characteristics in our approach allow us to probe distributions of self-generated $E+B$ fields, determine ρR by measuring the energy loss of backlighting protons, and sample all the implosion phases of an ICF spherical implosion. The radiographic data is contrasted to the x-ray images and hydrodynamic simulations. We note that earlier work by Mackinnon *et al.* [19] successfully demonstrated the feasibility of imaging implosions with protons (produced, in his case, by laser-plasma interactions), backlighting plastic (CH) capsules that were imploded by six 1-μm-wavelength laser beams. They reported no fields inside and surrounding the capsule, in contrast to the observations shown here, and this is not presently understood.

2. Experiments

The experiment is illustrated schematically in figure 1. A subject spherical CH capsule or a cone-in-shell target is driven directly with 36-40 beams of frequency-tripled (0.35 μm) UV light. The targets are ~ 860-μm in diameter, 20-24 μm thick shells and are all filled with 15-atm H_2 gas. The laser pulse is square, with duration of 1-ns and total energy ~ 14-16 kJ. The individual laser beams are smoothed using single-color cycle, 1 THz two-dimensional (2D) smoothing by dispersion (SSD) plus polarization smoothing (PS) [20,21].

Implosions are backlit with monoenergetic protons [fusion products from nuclear reaction D + ^{3}He $\rightarrow$ α + p (14.7MeV)], generated from D^{3}He-filled, exploding-pusher implosions, which are normally driven by 16 - 20 OMEGA laser beams [13,17,18]. The duration of the backlighter is ~ 130 ps, and the timing of the implosion laser is adjustable in different experiments relative to the times that the backlighting protons arrive at the implosions. The implosions are also imaged with self-emitted x rays from the directions nearly perpendicular to the backlighting protons by framing cameras.

In this approach, each individual image contains both spatial and energy information, because the CR-39 detectors record the position and energy of every individual proton. Such images can therefore be displayed to show either proton fluence versus position or proton mean energy versus position, providing important information about field distributions and capsule compression. Several sources of image broadening can compromise the fidelity of the radiography images, which are characterized by broadening radii R_p, R_{sc}, and R_d due to finite backlighter size (r_s), scattering at the subject (θ_{sc}), and broadening in the detector, respectively (r_d) [13]. The net effect of these individual processes is the convolution of the image structure by the Gaussian $\exp(-r^2/R_{\text{tot}}^2)$, where

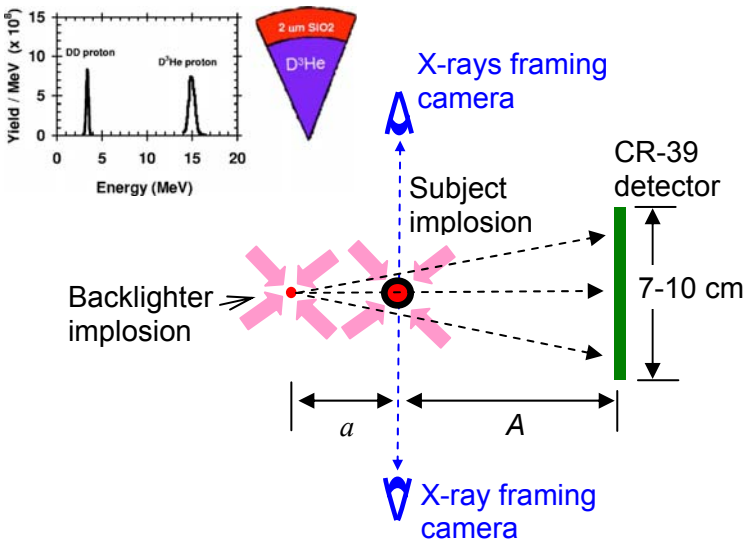

Figure 1. Experimental setup. Shown are the proton backlighter, subject implosion (either a spherical or a cone-in-shell target), imaging detectors, and x-ray framing cameras. Typical yields are ~2×10^8 for D^3He protons. A typical proton spectrum measured with a charged-particle spectrometer indicates that both nuclear lines are upshifted slightly from their birth energies because of capsule charging.

$R_{tot} = \sqrt{R_p^2 + R_D^2 + R_{sc}^2}$; and the characteristic image broadening radii $R_p = A(a + A)^{-1} r_s$, $R_{sc} = aA(a + A)^{-1}\theta_{sc}$, and $R_d = a(a + A)^{-1} r_d$. A and a are given in figure 1. The effective FWHM of the backlighter is ≈ 40 μm [13-18], and this is the primary limit on the intrinsic spatial resolution of the imaging system. In images of imploded capsules, spatial resolution is degraded somewhat by scattering of the imaging protons as they pass through the capsules.

3. Data

Figure 2 shows radiographic images of two snap shots made perpendicular to the Au cone axis with 15-MeV D^3He protons for cone-in-shell targets before and during implosion, proton fluence in figure 2a and energy in figure 2b, respectively. Several important features are apparent in these images. First, the character of the isotropic and monoenergetic proton source is reflected in the uniform background; second, a complex filamentary structure is seen in the fluence image of t =1.58 ns (this paper focuses on the region inside a target while the area outside this region is the subject of another study of external fields [22]). Third, substantial plasma blowoff from the cone casts a much wider shadow as the capsule is imploded. Fourth, a substantial enhancement of the proton fluence at the center of the imploded target suggests the presence of a radially-directed, focusing E field. And finally, radial compression of the capsule by a factor of two is seen in figure 2b. As a comparison, a time-integrated soft x-ray image taken using a pinhole camera is shown in figure 2c.

Figure 3 shows proton radiographs of spherical implosions at different times with proton fluence (figure. 3a) or mean proton energy (figure 3b). In the uncompressed case (0.0 ns) the protons that passed through the shell limb lost the most energy, resulting in the dark ring of part (b), and were scattered the most, resulting in the light ring of part (a). The soft x-ray images with ~ 60-ps step exposures taken using framing cameras are shown in figure 3c and indicate the temporal evolution of the size and shape of the capsule outer

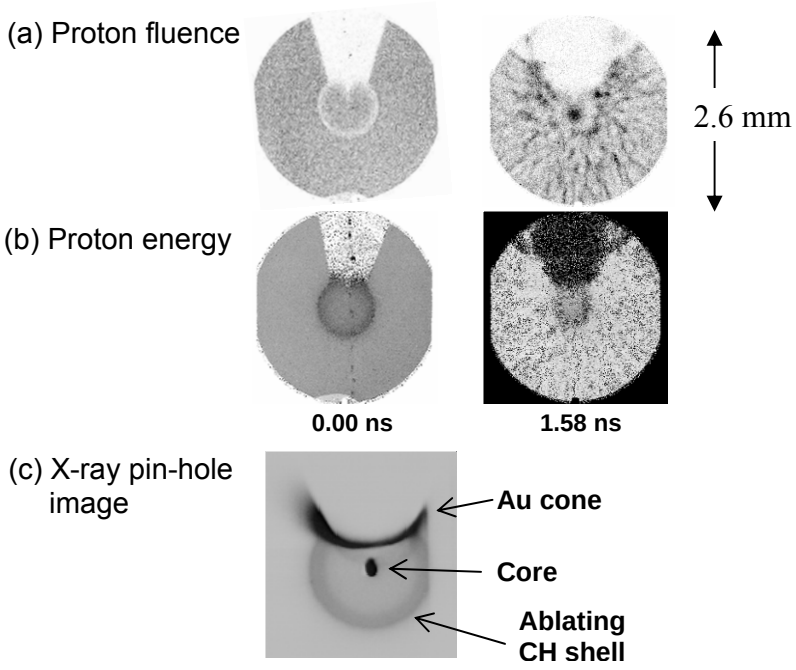

Figure 2: Images of proton fluence (a) and energy (b) of a spherical CH capsule with attached gold cone (at t = 0.0 and ~1.6 ns). In (a), darker means higher fluence, while in (b) darker means lower proton energy (more matter traversed). The gray-scale mapping is different for each image, to account for different backlighter yields and make the most important structure clearly visible. Figure 2(c) shows a time-integrated x-ray pinhole image.

boundary. A striking feature in figure 3a is that a strong central peak appears in the image during the early stage of implosion (t ~ 0.6 ns) while a central dip appears at later time (t ~ 1.6 ns). As shown in figure 4 from our other series of experiments [18], the lineouts of the two typical images (indicating the radial profiles of proton fluence,) provide the compelling evidence of such a fluence peak at an earlier time (t = 0.8 ns) and fluence dip at later time (t = 1.9 ns). To clearly demonstrate that these proton fluence peaks and dips do not depend on where the detector was placed, (*i.e.* at some special distances from the backlighter in the context of our experiment configuration,) we have conducted Monte Carlo calculations. The results shown in figure 5 indicate that for a giving amount of deflection, the focus or defocus of the image is relatively insensitive to the specific distance of the detector position.

3. Results and discussions

Two types of information of the implosion are able to be inferred from the above measured images: First, quantitative information about the implosion-associated fields through the spatial-distribution of proton fluence (fluence peak or dip due to deflections of proton trajectories). Second, quantitative information about capsule sizes (R) and areal densities (ρRs), as illustrated in figure 6. The details will be discussed as follows.

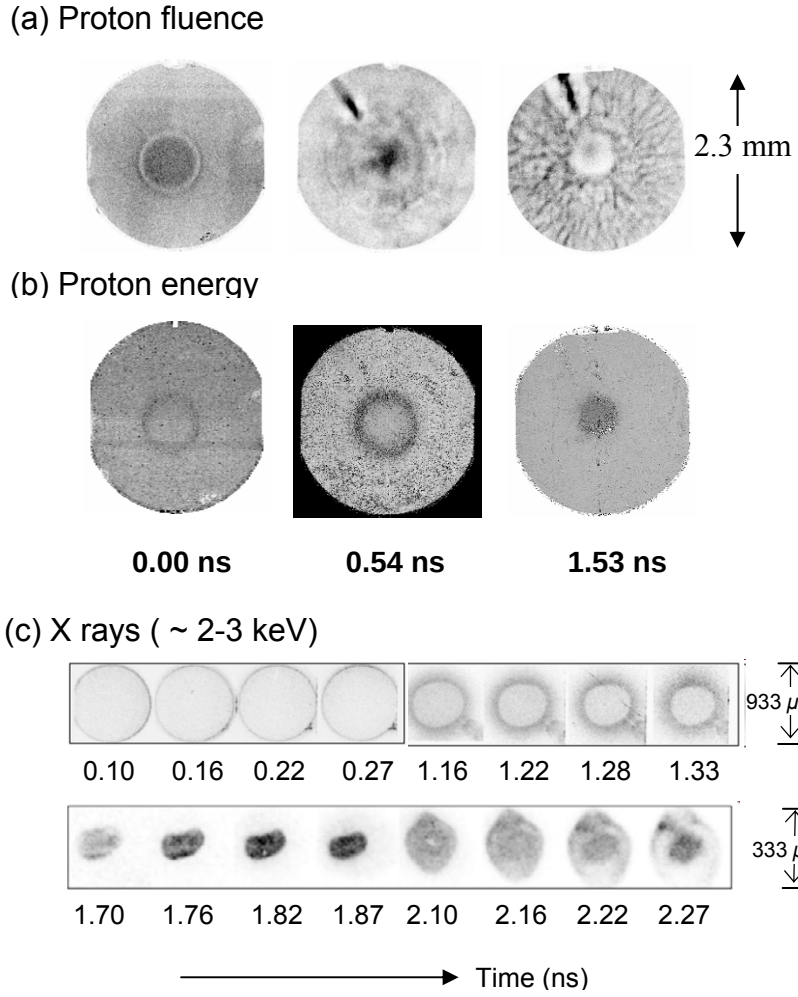

Figure 3. Proton radiographs of spherical implosions at different times, illustrating the time evolution of mass distribution and radial *E* field. The capsule-mounting stalk appears in the upper left corner of each fluence image. (c) The soft x-ray images with a ~ 60-ps step exposures, show the temporal evolution of the size and shape of the capsule outer boundary.

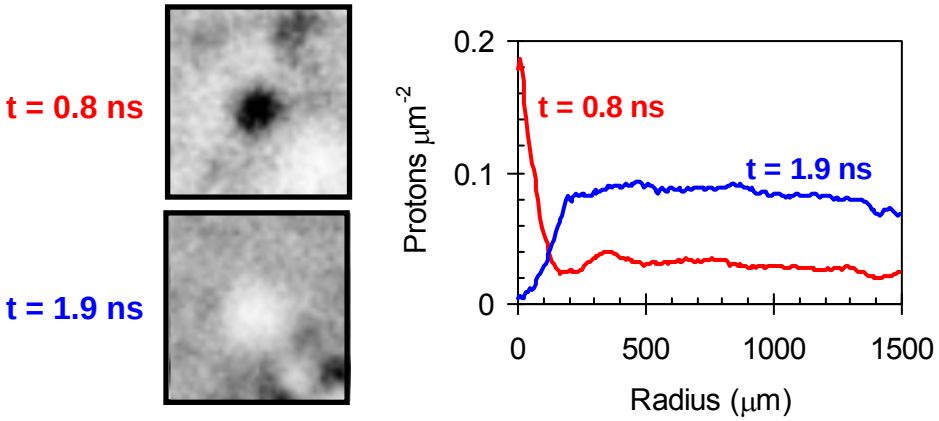

Figure 4. Radial profiles of the proton fluence images at t = 0.8 ns and 1.9 ns. A fluence peak occurs in the image centers during the early stages of implosion, indicating a "focusing" of imaging protons there; in contrast, the fluence is extremely low, or defocused, at the image centers at later times. Note that the different levels (×~2) of the proton fluence outside the capsules (r > ~ 200 μm) are due to the variations from the backlighter proton yields.

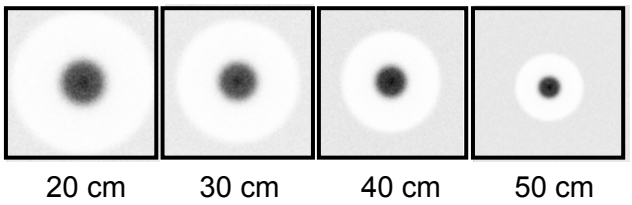

Figure 5. Monte-Carlo simulation of the proton fluence images at the detector plane at different distances. This shows that the observed effect of proton fluence peaked at the target center region is relatively insensitive to the specific distance of the detector position.

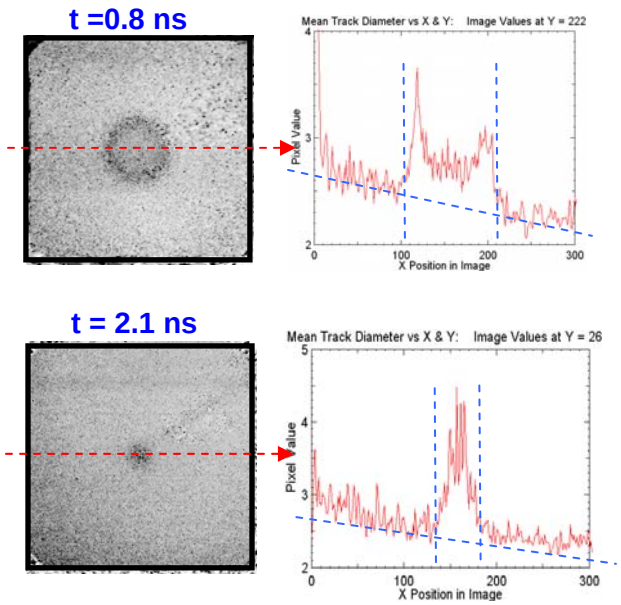

Figure 6. Illustration of lineouts through the centers of each of the individual images, the mean width provides the averaged capsule size (≈ 2R), while the mean height indicates the total ρL (≈ 2× ρR).

3a. A self-generated radial electric field

The striking features of proton fluence peak and dip demonstrated quantitatively in figure 4, as discussed below, cannot be accounted for as a consequence of proton scattering. These features must therefore result from the deflection of proton trajectories by radial electric fields. At earlier times the field must have been centrally directed in order to focus the protons passing within the capsule shell toward the center of the imaging detector. To account for the rapid change from a central fluence peak to a central fluence dip at ~ 1.5 ns, the radial field must have either reversed direction or suddenly become at least three times larger at that time (as shown by Monte Carlo simulations [18].), in which case all protons would have struck the detector outside the shadow of the capsule.

To demonstrate that radial fields are necessary to explain the central peaks and dips in image fluence, Monte Carlo simulations of image formation were conducted for the actual imaging geometry and backlighter yields, etc, using the density distributions predicted by hydrodynamic simulations. Images simulated with the assumption that there were no radial E fields, and that proton trajectories were deflected only by scattering occurring in the capsule shell limbs, are shown in figure 7 below. Although scattering does affect these images, it does not lead to peaks and dips of the sizes observed in the data. On

the other hand, images simulated with the assumption that there is a radial E field pointing to the center at t = 0.8 ns, but pointing away from the center at t = 1.9 ns, (and with the amplitudes,) are shown in figure 8 below. At t =0.8 ns there is a fluence peak in the center, while at t =1.9 ns there is fluence dip in the center. Both features basically mimic the experimental results above (figure 4), and provide compelling evidence that it is a radial E field, and its direction reversal. Note that these comparisons are qualitative and/or semi-quantitative because simulations are basically static while the measurements were dynamic within a period of time of the backlighter nuclear burn.

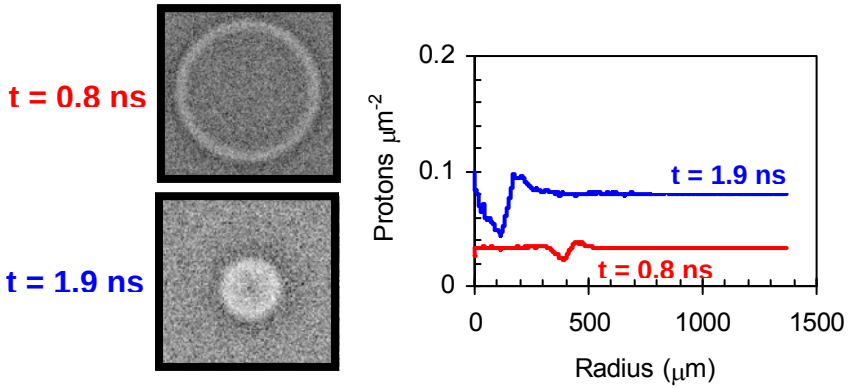

Figure 7. Monte-Carlo simulations proton fluence distribution caused by scattering only. It is shown that there is neither fluence peak at 0.8 ns nor fluence dip at 1.9 ns.

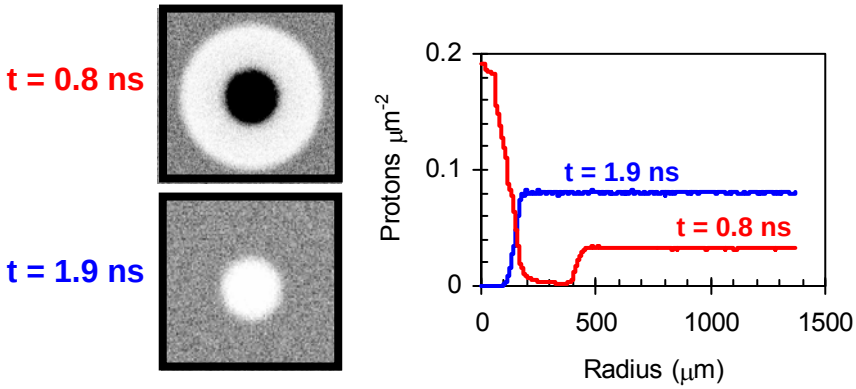

Figure 8. Monte-Carlo simulations (with scattering + radial E field; field direction reversed for t =1.9 ns). A fluence peak occurs in the image centers during the early stages of implosion, indicating a "focusing" of imaging protons there; in contrast, the fluence is extremely low, or defocused, at the image centers at later times. Note that the different levels (×~2) of the proton fluence outside the capsules (r > ~ 200 μm) are due to the variations from the backlighter proton yields.

The E-field source that is consistent with the data is the gradient of plasma electron pressure ($E \approx -\nabla p_e / e n_e$) [24] (other possible sources don't fit as naturally with the data [18]). The pressure gradient has the correct sign at earlier times, and reverses direction at approximately the correct time. This is illustrated by the electron pressure and density profiles from 0.8 ns to 2.1 ns, calculated using the LILAC hydro simulation program [25] and shown in figure 9. Using calculated ∇p_e and n_e at different times, we can estimate the

resultant strength of E as being in the range ~ -10^9 to ~ 10^8 V/m. The strength of such an E field can also be approximately estimated from the measured proton trajectory distortion [18]. The predictions match the data in three crucial ways: the field strength and sign before the reversal (~ -10^9 V/m, directed inward), the time of the field reversal (~1.5 ns), and the field strength after the reversal (~10^8 V/m directed outward). Note that the detailed structures of the fluence images are also modified, in ways that do not affect our conclusions, by the in-flight movement of the shell (V_{imp} ~ -2.5×10^7 cm/s), which is ~ 30 μm during the backlighter nuclear burn time (~ 130 ps.)

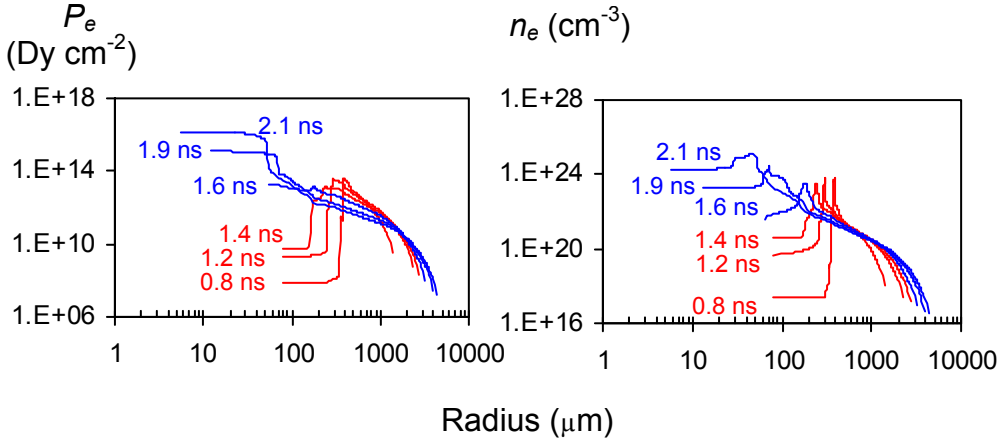

Figure 9. The profiles of the electron pressure at different times. It is shown that the gradients of the radial pressures are positive ($\nabla p_e > 0$) for early stages of implosions (t= 0.8, 1.2 and 1.4 ns), but are negative ($\nabla p_e < 0$) for later stages of implosions (t= 1.6, 1.9 and 2.1 ns).

3b. Areal density of implosion dynamics

Figure 3b shows the diameter-averaged D^3He proton images at different implosion times. The dark area represents the regions with lager proton diameters (and therefore lower energies) which resulted from the energy loss of protons passing through the different parts of an imploded capsule, leading to the determination of the target ρR [$\approx 0.5\rho L$, where $\rho L = \int_{E_0}^{E} \rho (dE/dx)^{-1} dE$ [26], and L is the proton path length]. As indicated in figure 6 that quantitative information about the sizes and ρRs at different times can be extracted from the lineout through the centers of individual images. The measurements are contrasted with LILAC simulations in figure 10 [18]. The simulations come reasonably close to matching the observed evolution of capsule convergence and ρR during the acceleration and coasting phases (~0-1.6 ns), but predict somewhat smaller values of radius, and larger values of ρR, than measured at the times of nuclear burn (~ 1.9 ns) and peak compression (~ 2.1 ns). Overall, this indicates that the implosions had approximately 1D performance, with little impact from hydrodynamic instabilities, before deceleration. It has been suggested that performance approaches 1D because of full single-beam smoothing, which significantly improves the shell integrity during the acceleration phase, and due to thickening of the shell during subsequent coasting which further enhances shell integrity [21]. The apparent degradation of capsule performance at later times relative to the 1D simulation may be largely a consequence of fuel-shell mixing and implosion asymmetry [10,11].

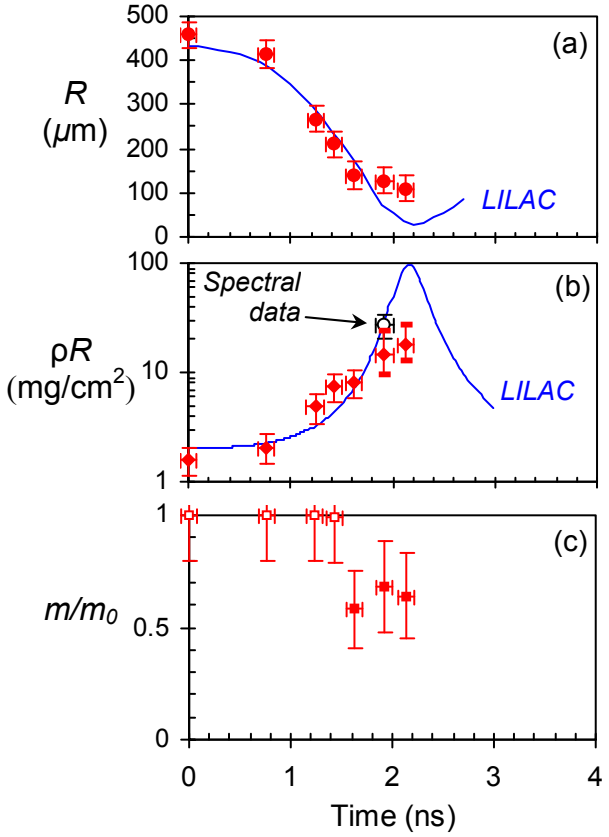

Figure 10. Measured capsule radius [solid cycles, (a)] and ρR [solid diamonds (b)] compared with LILAC 1D simulations (solid lines). The uncertainties in the x axis represent the nuclear burn time. ρRs at 1.9 and 2.1 ns in (b) are actually the lower limits, with large error bars resulting from the uncertainties of mean track diameters and the conversions to proton energy loss. Scattering plays an important role leading to such uncertainties. In contrast, the error bars at other times represent typical ρR asymmetries (~ ± 20%). A data point [open diamond in (b)] represents the mean $\rho R \approx 25$ mg/cm^2 (~ 90% of 1D calculation) at the bang time, as measured by several proton spectrometers in different directions. (c) Measured time-dependent mass ablations. The large error bars at the later times (solid squares) reflect the uncertainty of the above R and ρR measurements.

Proton data are qualitatively verified by x-ray images of self thermal emissions (~2 to 3 keV which allows full survey of target compression and rebound, see figure 3c). X-ray images shown that the shape of the outer boundary of a capsule evolves asymmetrically to form elongate images before the peak compression (~ 2.1 ns), then rebounds along the perpendicular direction. Since x-ray images are taken from the directions images nearly perpendicular to the backlighting protons, (and the proton images all had a round shape,) such an elongation suggests that the implosions were asymmetric as a result of more laser irradiation coming from poles than that from the equator. The sizes of x-ray images are slightly smaller than the sizes of proton image may indicate the effects of proton scattering.

Finally, the residual mass during the implosion process can be estimated in terms of the measured R and measured ρR: $m/m_0 \approx C_r^{-2}\, \rho R(t)/\rho R(0)$, where $C_r \equiv R(0)/R(t)$ is the target convergence ratio. Figure 11c indicates that ~ 30 - 40% of the shell has been ablated off by bang time. Although the mass estimates have large uncertainties due to their association with both R and ρR measurements, they are helpful for illustrating the dynamics of mass ablation during implosions.

4. Summary

In summary, we have conducted the first measurements of ICF implosion dynamics of spherical and cone-in-shell targets using time-gated, monoenergetic proton radiography. Critical information inferred directly from proton images uniquely characterizes the spatial structure and temporal evolution of imploded capsules that was hitherto unavailable using conventional measurements. To quantitatively delineate these measurements, data is contrasted with both self-emitted x rays and hydro simulations. Finally, variation of proton fluence inside the imploded targets during implosions unambiguously reveals the direction reversal of a self-generated radial electric field; this new observation is demonstrated to be a probable consequence of the reversal of the electron pressure gradient.

Acknowledgments

The work described here was performed at the LLE National Laser User's Facility (NLUF), and was supported in part by US DOE (Grant No. DE-FG03-03SF22691), LLE (subcontract Grant No.412160-001G), LLNL (subcontract Grant No.B504974), the Fusion Science Center at University of Rochester, and GA under DOE (DE-AC52-06NA27279).

REFERENCES

[1] Nuckolls J *et al* 1972 *Nature* **239**, 139
[2] Lindl J D, 1999 *Inertial Confinement Fusion* (New York: Springer-Verlag).
[3] Atzeni A and Meyer-Ter-Vehn J 2004 *The Physics of Inertial Fusion* (Oxford : Clarendon Press)
[4] McCrory R *et al* 2008 Phys. Plasmas **15**, 055503
[5] Tabak M *et a* 1994 Phys. Plasmas **1**, 1626
[6] Marshall F J *et al* 2004 Phys. Plasmas **11**, 251
[7] Craxton R S *et al* 2005 Phys. Plasmas **12**, 056304
[8] Séguin F H *et al* 2003 Rev. Sci. Instrum. **74**, 975
[9] Disdier L *et al* 2006 Phys. Plasmas **13**, 056317
[10] Li C K *et al* 2002 Phys. Rev. Lett. **89**, 165002
[11] Li C K *et al* 2004 Phys. Rev. Lett. **92**, 205001
[12] Soures J M *et al* 1996 Phys. of Plasmas **3**, 2108
[13] Li C K *et al* Rev. Sci. Instrum. **77**, 10E725
[14] Li C K *et al* 2006 Phys. Rev. Lett. **97**, 135003
[15] Li C K *et al* 2007 Phys. Rev. Lett. **99**, 015001
[16] Li C K *et al* 2007 Phys. Rev. Lett. **99**, 055001
[17] Rygg J R *et al* 2008 Science **319**, 1223
[18] Li C K *et al* 2008 Phys. Rev. Lett. **100**, 225001
[19] Mackinnon A *et al* 2006 Phys. Rev. Lett. **97**,045001
[20] Skupsky S *et al* 1999 Phys. Plasmas **6**, 2157
[21] Meyerhofer D D *et al* 2001 Phys. Plasmas **8**, 2251
[22] Séguin F H *et al.*, paper in preparation.
[23] Highland V L 1975 Nucl. Instrum. Methods **129**,497
[24] Braginskii S I 1965 *Review of Plasma Physics* (New York: Consultant Bureau)
[25] Deletrezz J *et al* 1987 Phys. Rev. A **36**, 3926
[26] Li C K and Petrasso R D 1993 Phys. Rev. Lett. **70**, 3059
[27] Li C K *et al* 2000 Phys. Plasmas **7**, 2578